This article has been accepted for publication in a future issue of this journal, but has not been fully edited. Content may change prior to final publication. Citation information: DOI 10.1109/TCSVT.2018.2859792, IEEE Transactions on Circuits and Systems for Video Technology

Improving pairwise PEE via hybrid-dimensional histogram generation and adaptive mapping selection

Bo Ou, Xiaolong Li, Weiming Zhang, and Yao Zhao, *Senior Member, IEEE*

***Abstract*—Pairwise prediction-error expansion (pairwise PEE) is a recent technique for high-dimensional reversible data hiding. However, in the absence of adaptive embedding, its potential has not been fully exploited. In this paper, we propose the adaptive pixel pairing (APP) and the adaptive mapping selection for the enhancement of pairwise PEE. Our motivation is twofold: building a sharper two-dimensional (2D) histogram and designing the effective 2D mapping for it. In APP, we consider to increase the similarity between pixels in a pair, by excluding rough pixels from pairing and only putting the smooth pixels into pairs. In this way, the pixels in a pair have a larger possibility of being equal, and thus the resulted 2D prediction-error histogram (PEH) has a lower entropy. Next, the adaptive mapping selection mechanism is introduced to properly determine the optimal modification, based on "whether it fits for the resulted PEH" rather than by the heuristic experience. The experimental results show that the proposed method has a significant improvement over the pairwise PEE.**

***Index Terms*—Reversible data hiding, pairwise prediction-error expansion, adaptive pixel pairing, 2D histogram modification.**

I. Introduction

Reversible data hiding (RDH) is a branch of digital watermarking to deal with the secret message transmission for sensitive image processing [1]. The word *reversible* denotes the perfect recovery of both the original content and the hidden data. As such, RDH can be intensively used in a variety of secure applications, say, law enforcement, archive management, image authentication, etc. In literature, three categories of RDH methods can be distinguished: (1) compression based methods [2]–[7], (2) histogram modification based methods including histogram shifting (HS) [8]–[13], difference expansion (DE) [14], [15] and prediction-error expansion (PEE) [16]–[30], and (3) integer transform based methods [31]–[34].

Recently, the interest in the field of RDH has been renewed due to the new perspectives about adaptive embedding [10], [17], [19], [21], [22], [25], [28], [35]–[37], in which the data embedding differs from one image/region to another and calls for a finer modification depending upon the content. Among them, a new derived RDH technique, namely pairwise prediction-error expansion (pairwise PEE) [25], is proposed to consider every two pixels jointly for data embedding, and has been verified effective in reducing the embedding distortion for low capacity. In the method, every two neighboring pixels in a diagonal or anti-diagonal direction are combined into a pair. Such pairing is based on the assumption that, the nearby pixels usually have similar intensities and so the similarity between pixels can be indicated by their spatial distance. By utilizing the similarities between the neighboring pixels, the two-dimensional prediction-error histogram (2D PEH) has a lower entropy than the one-dimensional (1D) PEH and then a more effective modification manner can be designed.

Although pairwise PEE has demonstrated an improved performance compared with the conventional 1D methods, the issues about 2D histogram generation and adaptive 2D histogram modification still need to be investigated. In the latest work [28], Dragoi and Coltuc proposed a novel pixel pairing to classify the prediction-errors into three categories at first, and then combine the pixels of a specific category into pairs. The pairing starts in a pixel-wise manner, and each pixel finds its partner within the category. This strategy helps to form the sharply distributed 2D PEH, and thus an improvement is obtained over [25]. In view of the measurement for pixels' similarities, both [25] and [28] adopt the spatial correlations to stimulate the similarity of pixels. However, the pixel similarity may not be simply characterized by the spatial distance, and the imperfect pairing would result from the structure and the edge of an image. Besides, designing a content-based mapping is still a blank, as the current 2D mappings are empirically designed but not adaptively determined.

In this paper, within the framework of pairwise PEE, we propose two new techniques for histogram generation and modification, called adaptive pixel pairing (APP) and adaptive mapping selection respectively, to further improve the high-dimensional PEE. Unlike the previous works, during the histogram generation, the proposed APP rejects the large-magnitude prediction-errors for pairing, and only uses the prediction-errors near zero to generate the 2D PEH. The pixel pairing is determined by the intensity, and has nothing to do with the spatial distances between pixels. As only the smooth pixels are utilized, the derived 2D PEH has a lower entropy, and is helpful for a low-distortion data embedding. The optimal 2D mapping is then determined to modify the small-

B. Ou is with the College of Computer Science and Electronic Engineering, Hunan University, Changsha 410082, China (e-mail: oubo@hnu.edu.cn).

X. Li and Y. Zhao are with the Institute of Information Science, Beijing Jiaotong University, Beijing 100044, China (e-mail: {lixl,yzhao}@bjtu.edu.cn.

W. Zhang is with the CAS Key Laboratory of Electromagnetic Space Information, University of Science and Technology of China, Hefei 230026, China (e-mail: zhangwm@ustc.edu.cn).

This work was supported by the National Key Research and Development of China (No. 2016YFB0800404), the National Science Foundation of China (Nos. 61502160, 61572052, U1736213 and 61332012), and the Fundamental Research Funds for the Central Universities (No. 2017RC008).

magnitude prediction-errors in the pairwise manner, which is content-based and thus well suited to the 2D PEH. For the rough pixels, we use them to form a 1D PEH and only perform the shifting operation on them in the pixel-wise manner for the sake of reversibility. Experimental results demonstrate that the proposed method can improve the performance of pairwise PEE, and also yield a better performance than some state-of-the-art methods.

The main contribution of this paper is the hybrid framework of 2D and 1D PEE that we formulate, which goes beyond the simple PEE, and encapsulate the following two aspects:

- a hybrid histogram generation mechanism, allowing the 1D and 2D PEHs to carry out the RDH jointly,
- and an effective adaptive 2D mapping selection to make the histogram modification manner suited to the resulted PEH, while releasing the computational complexity.

The rest of paper is organized as follows. The framework of pairwise PEE is briefly reviewed in Section II. Then, Section III presents the proposed method in details, and analyzes its benefit. The experimental results are given and discussed in Section IV, and the conclusions are drew in Section V.

II. Pairwise PEE framework

We first briefly review the pairwise PEE [25] to show how PEE is represented in the 2D space, and then describe the advantages of transforming RDH in the high dimensional space. Since pairwise PEE is based on the double-layer embedding and the two layers are processed in a similar way, we only take the single layer's embedding for illustration.

Firstly, the pixels of a single layer are collected as a sequence $(p_1, ..., p_N)$ according to a specific scanning order. Then, the prediction-errors between the pixels and their estimates are obtained for data embedding, where the prediction-error sequence is denoted as $(e_1, ..., e_N)$. Because the prediction decorrelates the image, the derived prediction-errors are more efficient in data embedding than the original pixels. Next, like the other PEE-based methods, pairwise PEE consists of two major steps, namely histogram generation and histogram modification.

In the first step, the frequencies of prediction-errors are counted to derive the PEH, which reflects the statistical property of image content and varies from one to another. The PEH is the basis of PEE-based RDH, and the difference between the pairwise PEE and the conventional one lies in whether the prediction-errors are jointly modified or not. In the conventional PEE, the prediction-errors are modified one by one, and so the modifications on them are independent. Taking the case of $T = 1$ for illustration (T denotes the maximum modification on a pixel), a prediction-error e_i is modified in four cases below.

- If $e_i = 0$, then the marked prediction-error is $e'_i = e_i + b$, where $b \in \{0, 1\}$ is a binary bit.
- If $e_i = -1$, then $e'_i = e_i - b$.
- If $e_i > 1$, then $e'_i = e_i + 1$.
- If $e_i < 0$, then $e'_i = e_i - 1$.

With the help of invariant prediction, the modification on a prediction-error can be correctly retrieved, and the marked

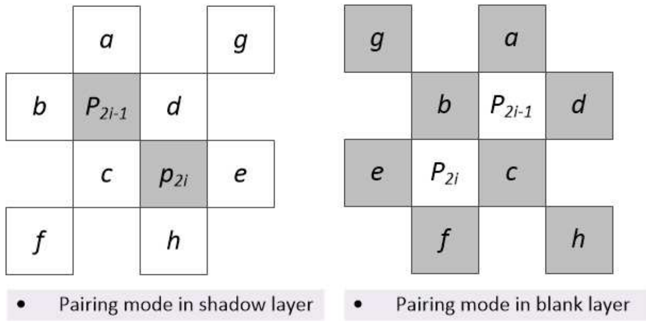

Fig. 2. Pairing modes for the shadow and the blank layers. Here, every two neighboring pixels in the diagonal or anti-diagonal direction are combined into a pair.

pixel value is obtained as $p'_i = p_i + e'_i$. Since the above modification is conducted in a pixel-wise manner, the PEH manipulated in data embedding is 1D and defined as

$$h_1(k_1) = \#\{i : e_i = k_1\} \tag{1}$$

where $\#$ returns the cardinality of a set. In essence, the transformation between the original PEH and its marked PEH can be simply represented as a mapping. The 1D mapping is shown in the left sub-figure of Fig. 1. For pairwise PEE, every two neighboring prediction-errors are jointly counted, and the 2D PEH $h_2(k_1, k_2)$ is

$$h_2(k_1, k_2) = \#\{i : e_{2i-1} = k_1, e_{2i} = k_2\}. \tag{2}$$

When viewed in this higher dimensional space, it is interesting to find that a further improvement can be obtained by exploiting the high order correlations, and a lower entropy of PEH is obtained [25]. In this case, the reversible mapping is changed into a 2D form as shown in the right sub-figure of Fig. 1.

In the second step, a special design is that pairwise PEE embeds a less amount of bits into the most smooth pairs in exchange of distortion reduction. One factor affecting the exchange is the number of smooth pairs, which is determined by the way of pixel pairing. According to the common experience, the nearest pixels are more correlated. So, the pixel combination is designed to pair up the nearest two together as shown in Fig. 2. For a pixel pair $\mathbf{p_i} = (p_{2i-1}, p_{2i})$, its prediction context contains eight pixels $\{a, b, ..., f\}$ which belong to the other layer. Then, according to the rhombus prediction, the prediction-error pair $\mathbf{e_i} = (e_{2i-1}, e_{2i})$ is computed as

$$\begin{cases} e_{2i-1} = p_{2i-1} - \lceil (a + b + c + d)/4 \rceil \\ e_{2i} = p_{2i} - \lceil (c + d + e + f)/4 \rceil \end{cases} \tag{3}$$

where $\lceil \cdot \rceil$ denotes the ceiling function. To preferentially process the smooth pairs, the noise level is introduced to measure the local complexity for the pair. Formally, the noisy level NL_i for the pair $\mathbf{e_i}$ is calculated as

$$\begin{aligned} NL_i = &|a - b| + |b - c| + |c - d| + |d - a| + \\ &|c - f| + |f - e| + |e - d| + |d - g| + |c - h| \end{aligned}. \tag{4}$$

After that, a new 2D mapping is employed as shown in Fig. 3, where the new mapping is compared with the conventional one for illustration. Note that only the first quadrant is compared

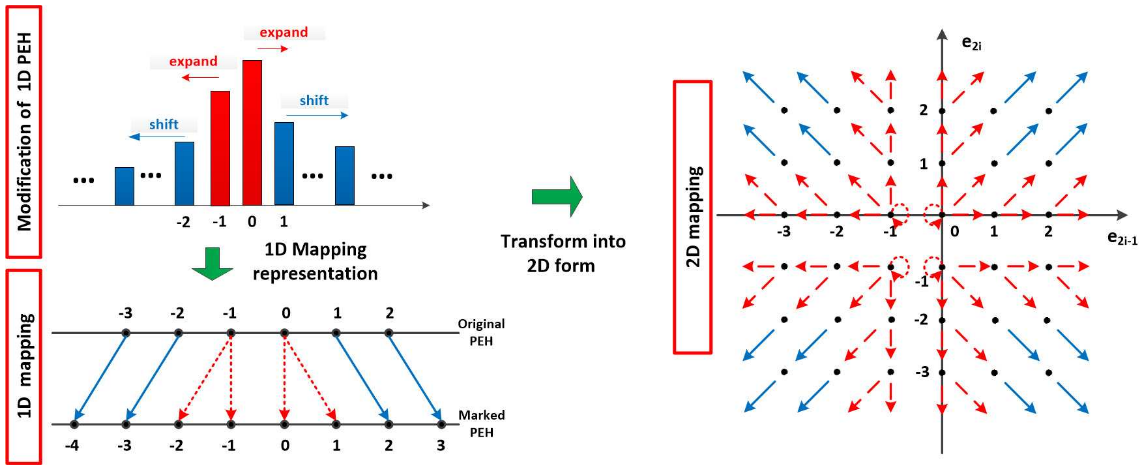

Fig. 1. Representations of the data embedding in the conventional PEE from the 1D and 2D views.

as the other three quadrants employ the similar 2D mappings. Compared with the conventional PEE, the difference is that, by discarding the large-distortion modification from $(e_{2i-1}, e_{2i}) = (0, 0)$ to $(e'_{2i-1}, e'_{2i}) = (1, 1)$, the pair $(0, 0)$ is only mapped to $(0, 0)$, $(0, 1)$ or $(1, 0)$, respectively, and thus is embedded with $log_2 3$ bits instead of 2 bits. The benefit is that the total embedding distortion will be reduced, and the experimental results also show that the capacity is equaled to or larger than the conventional one.

However, the drawback of pairwise PEE is that the pixel combination and the employed 2D mapping are not adaptive. Once designed, the pixel pairing and the 2D mapping are fixed no matter how the image's characteristics vary. On one hand, a better pairing mode can be achieved by considering the smooth prediction-errors first. On the other hand, the optimal 2D mapping should be adapted to the statistical characteristics of PEH, and seeks to minimize the distortion while preserving the capacity. Of course, the computational price paid for the adaptation must be affordable. This requires a reasonable optimization strategy designed by the sophisticated encoder.

Before introducing our scheme, we give an example to show how the pixel pairing affects the capacity and the distortion. The data in the example is artificial and only used to illustrate the possibly better pairing. Suppose that there are four prediction-errors “0, 8, 1, 10” with the spatial indices “1, 2, 3, 4”. In [25], the four prediction-errors are combined into two pairs $(0, 8)$ and $(1, 10)$ sequently, with the index pairs of $(1, 2)$ and $(3, 4)$. The two pairs could be embedded with 2 bits, and the total distortion is 3. But if we restrict the to-be-combined prediction-errors to be no larger than 1, only one pair would generate and the derived pair is $(0, 1)$ with the index pair $(1, 3)$. Because the unused prediction-errors “8, 10” usually have the large noise levels, they will be skipped during data embedding. In this ideal case, the capacity by using the one pair is the same as that of two pairs, but the distortion is reduced to $3/2$. Similarly, in another example, when two pairs $(1, 5)$ and $(1, 6)$ are reduced to $(1, 1)$ by using the new pairing, not only the gain is obtained in distortion reduction from 2 to 1, but also in capacity increase from 0 to 1.

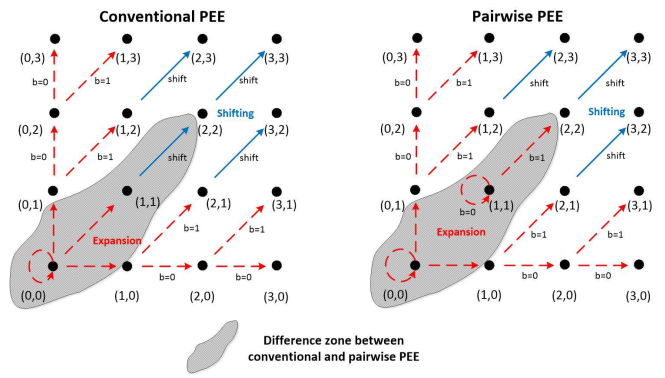

Fig. 3. 2D mapping comparison for the conventional and the pairwise PEE in the first quadrant. The difference in design is marked with gray.

III. Proposed Method

We propose to further improve the pairwise PEE from two aspects: 1) construct a sharper 2D PEH and 2) design an effective 2D mapping for it. The framework of the proposed embedding is given in Fig. 4. It is a hybrid procedure of 1D and 2D modifications, and aims to inherit the advantages of pairwise PEE for a low embedding distorion. We use the APP strategy to select the most suitable prediction-errors for the 2D PEH generation, and take the rest of ones to form a 1D PEH. Here, the 2D PEH consists of the small-magnitude prediction-errors, and the 2D mapping for it is adaptively chosen. While, the 1D PEH contains the large-magnitude prediction-errors, and is modified by the conventional 1D mapping to guarantee the reversibility.

A. Pixel pairing for 2D PEH generation

Besides designing an effective 2D mapping, an advanced histogram generation offers the most immediate way for performance enhancement. This is because that a sharply distributed PEH consists of more expandable pairs near zero, and a given capacity can be satisfied with a low cost in shifting the pixels. For pairwise PEE, a better PEH generation could be accomplished by increasing the similarity of pixels within a pair.

This article has been accepted for publication in a future issue of this journal, but has not been fully edited. Content may change prior to final publication. Citation information: DOI 10.1109/TCSVT.2018.2859792, IEEE Transactions on Circuits and Systems for Video Technology

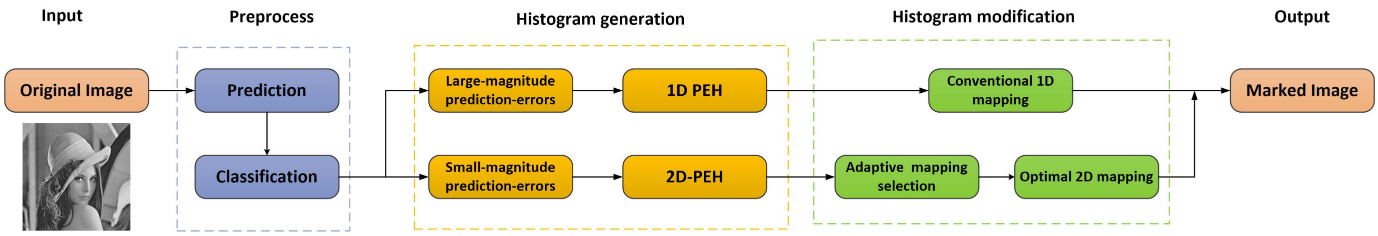

Fig. 4. Flowchart of the proposed method, where the large- and small-magnitude prediction-errors are modified in the 1D and 2D manners, respectively.

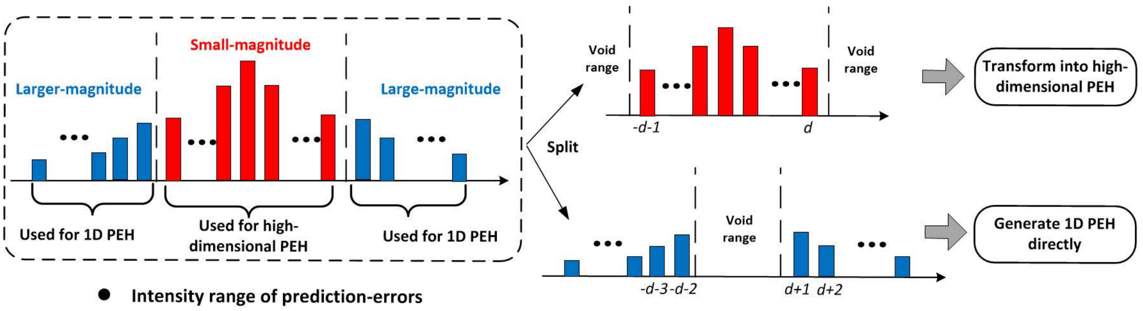

Fig. 5. General idea for the proposed method using the hybrid PEHs of 1D and high dimensional, where the small-magnitude prediction-errors are used to constitute the higher dimensional PEH in order to better exploit the high-order correlations.

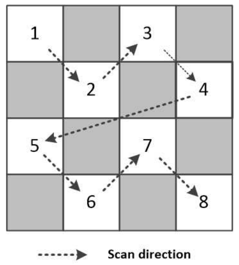

Fig. 6. Scanning order for a single layer.

To this end, we propose to combine the similar prediction-errors into pairs based on their intensities, and construct two independent PEHs. The main idea for the proposed histogram generation is given in Fig. 5. In the general form of hybrid histogram generation, the prediction-errors are classified into the smooth and the rough sets respectively as

$$\begin{cases} S_{(-d-1,d)} = \{e_i : -d-1 \leq e_i \leq d\} \\ R_{(-d-2,d+1)} = \{e_i : e_i \leq -d-2 \text{ or } e_i \geq d+1\} \end{cases} \tag{5}$$

and only the ones falling into the intensity range $[-d-1, d]$ (i.e., the set $S_{(-d-1,d)}$) are utilized to form the high dimensional PEH. The motivation is to better exploit the correlations within the smooth pixels, because these prediction-errors has a higher correlation than the others. To verify this, we compare the entropies of the 2D PEHs derived from the prediction-errors of different intensity ranges. Table I shows the results. It is observed that the 2D PEH derived by the small magnitude prediction-errors yields a lower entropy than the original 2D PEH, and the more smooth the pixels, the lower entropy is obtained. Based on the well-known commonsense, the low-entropy PEH will be beneficial for efficient RDH. In our method, the parameter of hybrid histogram generation is set as $d = 1$. It means that only the prediction-errors within the range of $[-2, 1]$ are combined into pairs.

Except the pairing manner, the proposed scheme adopts the same mechanism as [25], including the double layer embedding, the rhombus prediction (3) and the noise level definition (4). Denote the pixel's noise level as n_i. According to the pairing mode in Fig. 2, every two neighboring pixels p_{2i-1} and p_{2i} share the same noise level of pair, i.e., $n_{2i-1} = n_{2i} = NL_i$ in (4). By setting a threshold t, the smooth enough pixels with $n_i < t$ are collected, and then sorted based on the scanning order. For simplicity, the derived prediction-error sequence is still denoted as $(e_1, .., e_N)$, where N is the number of pixels with $n_i < t$. The prediction-errors are classified into the smooth and the rough sets respectively as

$$\begin{cases} S_{(-2,1)} = \{e_i : -2 \leq e_i \leq 1\} \\ R_{(-3,2)} = \{e_i : e_i \leq -3 \text{ or } e_i \geq 2\}. \end{cases} \tag{6}$$

In this way, the large-magnitude prediction-errors are excluded for pairing, and the pair sequence is created by combining the small-magnitude ones. The prediction-errors of the set $S_{(-2,1)}$ are combined into pairs in an ascending scan order as $((e_{\sigma(1)}, e_{\sigma(2)}), ..., (e_{\sigma(2m-1)}, e_{\sigma(2m)}))$, where $2m$ is the cardinality of $S_{(-2,1)}$ and σ is a mapping function from $\{1, ..., 2m\}$ to $\{1, ..., N\}$ such that $\sigma(1) < ... < \sigma(2m)$. For better illustration, an example for the generation of the pair sequence is given in Fig. 7. In addition, to show the effectiveness of this hybrid histogram generation, we conduct a comparison between the entropies of the conventional and the hybrid PEHs. Denote the entropies of the proposed 1D and 2D PEHs as E_1 and E_2, respectively. The entropy H_{hybrid} for the hybrid PEH is a weighted average value, and computed as

$$H_{hybrid} = \frac{H_1 \times \eta_1 + H_2 \times \eta_2}{\eta_1 + 2 \times \eta_2} \tag{7}$$

where η_1 and η_2 are the numbers of the pixels in 1D PEH and the pixel pairs in 2D PEH, respectively. The weighted

This article has been accepted for publication in a future issue of this journal, but has not been fully edited. Content may change prior to final publication. Citation information: DOI 10.1109/TCSVT.2018.2859792, IEEE Transactions on Circuits and Systems for Video Technology

TABLE I
ENTROPIES OF 2D PEHS DERIVED FROM DIFFERENT INTENSITY RANGES. THE INTENSITY RANGES OF $[-\infty,+\infty]$, $[-5,4]$ AND $[-2,1]$ ARE OBTAINED BY USING THE PARAMETER $d=\infty$, $d=4$ AND $d=1$, RESPECTIVELY.

Intensity range	Airplane	Baboon	Barbara	Boat	Elaine	Lake	Lena	Peppers
$[-\infty,+\infty]$	7.485	11.627	9.635	9.459	9.708	9.768	8.067	8.917
$[-5,4]$	4.961	6.036	6.056	4.812	4.690	4.931	4.546	4.429
$[-2,1]$	3.869	3.998	3.988	3.997	3.991	3.990	3.986	3.997

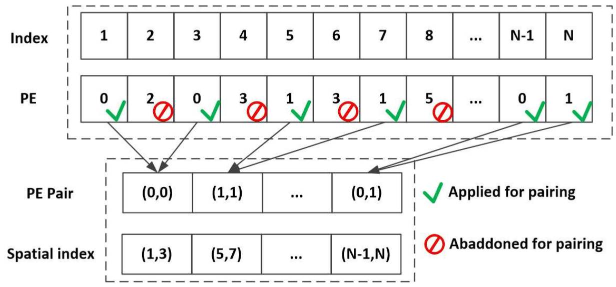

Fig. 7. An example of of the proposed APP, where the prediction-error pair sequence is a result of trimming off the original prediction-error sequence, and the large-magnitude prediction-errors are all excluded from pixel pairing.

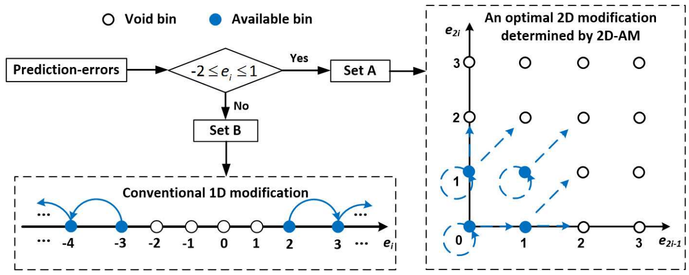

Fig. 8. The proposed data embedding includes both 1D and 2D modifications, and the modification on a prediction-error is determined by the intensity. Note that the 1D modification is fixed, but the optimal 2D mapping is adaptively determined by the 2D PEH.

average entropy is defined to measure the average amount of information carried by a prediction-error in the hybrid PEH. In the denominator part of (7), the pair number η_2 is multiplied by 2 to obtain the number of prediction-errors in the 2D PEH. The detail of entropy comparison is given in Table II. By the table, it is seen that the entropy of ours is lower than the conventional pairwise PEE. In other words, the proposed histogram generation better decorrelates the image and is more helpful for the efficient RDH.

After the histogram generation, the data embedding is proceeded as shown in Fig. 8, where the prediction-errors of the sets S and R are modified by 2D and 1D mappings, respectively. For a pair in the set S, it is modified in a pairwise manner according to a specific 2D mapping Θ, which will be determined by the optimal mapping selection (see the latter description of III-B). For the prediction-errors in the set R, we use the conventional 1D mapping to substrate or add them by 1, i.e.,

$$e_i' = \begin{cases} e_i+1, & \text{if } e_i \ge 2 \\ e_i-1, & \text{if } e_i \le -3 \end{cases} . \tag{8}$$

The reversibility of the hybrid embedding is based on the correct classification of prediction-errors both at encoder and decoder. Because the maximum modification on a pixel is restricted to 1, the original intensity range of prediction-error in the set $S_{(-2,1)}$ is $[-2,1]$, and the range for the marked prediction-errors is $[-3,2]$ after embedding. While, for the prediction-errors in $R_{(-3,2)}$, the ranges before and after embedding are $(-\infty,-3]\cup[2,+\infty)$ and $(-\infty,-4]\cup[3,+\infty)$, respectively. As a result, at the decoder, the marked sets $S'_{(-2,1)}$ and $R'_{(-3,2)}$ are classified as

$$\begin{cases} S'_{(-2,1)} = \{e_i' : -3 \le e_i' \le 2\} \\ R'_{(-3,2)} = \{e_i' : e_i \le -4 \text{ or } e_i \ge 3\} \end{cases} . \tag{9}$$

There is no overlap between the sets $S'_{(-2,1)}$ and $R'_{(-3,2)}$ at decoders. Hence, the correct classifications for the marked ones can be guaranteed, and no side information for this classification is required. Within the set, the reversibility is ensured by the employed reversible mapping. That is, the original prediction-errors are recovered from the marked ones by using the corresponding mapping inversely.

Seen from another point of view, the proposed histogram generation is a matter of transforming the conventional pair sequence of pairwise PEE into a reduced one. For ease of understanding, we take the non-negative prediction-errors for illustration, and mark them with three types according to the intensity: "0", "1" and "z", where $z>1$. Besides, the ingredient of prediction-error pair (a,b) or (b,a) is denoted as $\{a,b\}$. Since the proposed APP only combines a small number of prediction-errors into the pair sequence, it can be viewed as a process of recombining the conventional pairs of [25], where some two pairs of [25] are reduced into only one in the proposed method. Specifically, compared with the conventional pairing, the recombination process has the following three transformations, including

- $\{0,z\}+\{0,z\} \Rightarrow \{0,0\}$.
- $\{1,z\}+\{1,z\} \Rightarrow \{1,1\}$.
- $\{0,z\}+\{1,z\} \Rightarrow \{0,1\}$.

where two pairs on the left are recombined into the right one in the 2D PEH, as the z is abandoned for pairing. It is possible for the distributed smooth pixels to be combined into pairs without the restriction of spatial distance. We observe the data embedding on the first 30 prediction-errors on Lena to compare the capacity and distortion by using [25] and ours, where the 2D mapping is used as the one in [25]. The comparison is shown in Fig. 9. It is seen that, the proposed method can not only increase the capacity, but also reduce the distortion. Combined with the results in Table II, it is verified that the proposed APP indeed improves the pairwise PEE. In fact, the benefit would be increased when the low noise level is utilized. In that case, it is easier to make large-magnitude

This article has been accepted for publication in a future issue of this journal, but has not been fully edited. Content may change prior to final publication. Citation information: DOI 10.1109/TCSVT.2018.2859792, IEEE Transactions on Circuits and Systems for Video Technology

TABLE II
HISTOGRAM ENTROPY COMPARISON BETWEEN THE CONVENTIONAL PAIRWISE PEE AND THE PROPOSED METHOD. BY TAKING BOTH THE 1D AND 2D PEHS INTO ACCOUNT, THE ENTROPY OF THE PROPOSED METHOD IS CALCULATED ACCORDING TO (7).

Images	Airplane	Baboon	Barbara	Boat	Lake	Lena
Conventional	3.742	5.813	4.818	4.729	4.884	4.034
Proposed	2.904	5.323	4.150	3.925	4.113	3.108

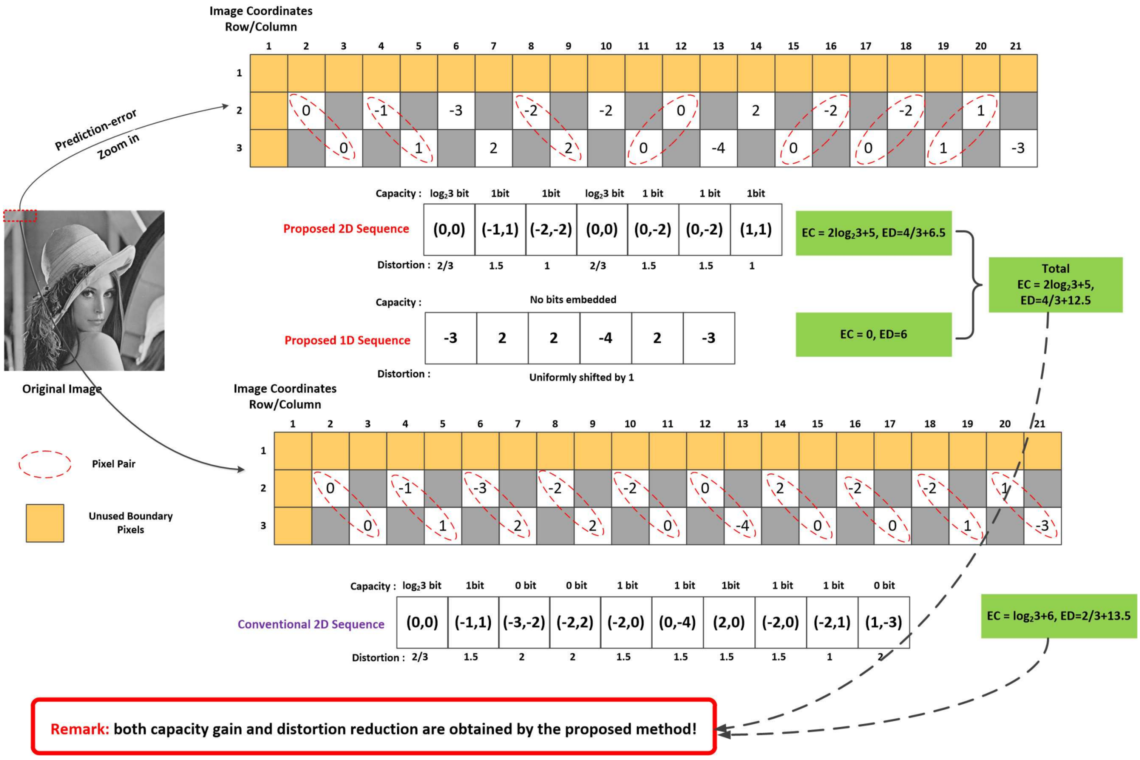

Fig. 9. Comparison in terms of the pixel pairing between the proposed method (upper) and the pairwise PEE (bottom) on Lena image. Here, the first 30 prediction-errors in the upper-left of Lena image are given for comparison.

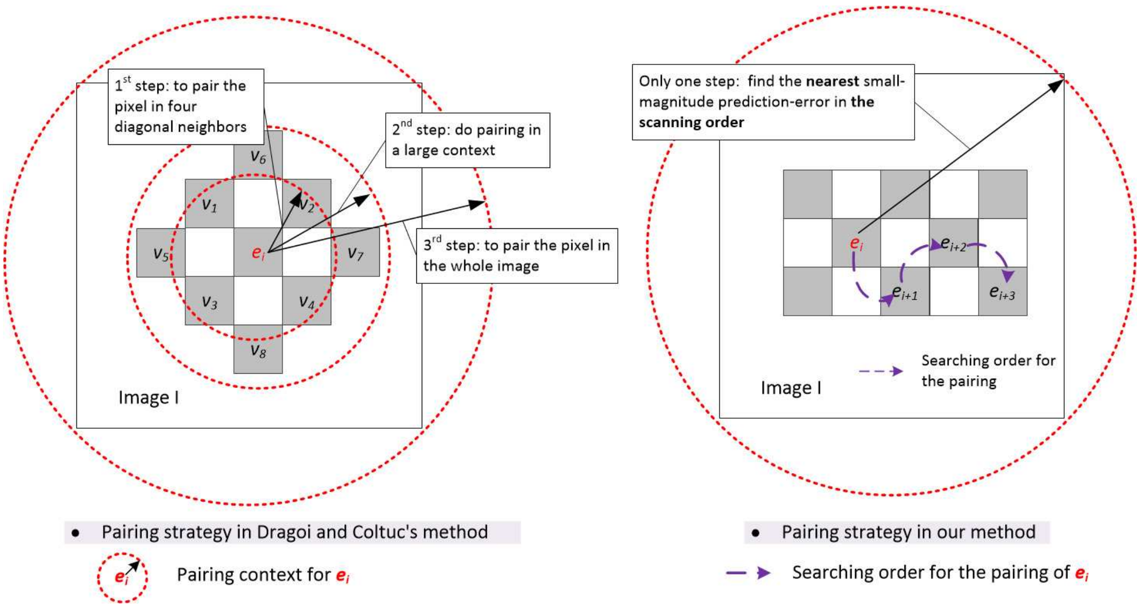

Fig. 10. Comparison in the adaptive pixel pairing strategy for the proposed method and Dragoi and Coltuc's method [28], where v_1, ..., v_8 denote the prediction-errors in the context specified by [28].

prediction-errors unprocessed.

Before further introducing the proposed design in histogram modification, we simply illustrate the difference of APP s-trategy compared with that of Dragoi and Coltuc's method [28]. Both the proposed method and [28] consider to limit the pairing of two prediction-errors by the intensity, however, there still exit some differences as follows.

- The pixel pairing in [28] is not determined by intensity, but also related to the distance between pixels. It employs a three-step pairing mechanism as shown in Fig. 10, which first combines the small-magnitude prediction-errors in a local context, and then gradually extends the paring range. More specifically, a small-magnitude prediction-error will first search another small-magnitude one within a small local context (including four diagonal prediction-errors v_1, v_2, v_3 and v_4). If it fails to find the partner, it continues to search in a larger context in the second step, which additionally includes v_5, v_6, v_7, and v_8. If it fails again, it will be left temporally as a remaining to-be-paired one. At last, all the remaining prediction-errors will be paired two by two in a scanning order. In summary, for a pixel, the search stops until the current pixel is successfully paired.
- In contrast with [28], the strategy of the proposed method is straightforward. We combine every two small-magnitude prediction-errors in a scanning order, and the pixel pairing is finished in one step. By the comparison, it can be found that the APP algorithms in ours and [28] are different. For a pixel's pairing, the method [28] gives a higher priority for the eight nearest neighbors (four in diagonal direction and the other four in the horizontal/vertical directions), but the proposed method just finds the nearest small-magnitude prediction-error according to the scanning order.

As a result, the two APP strategies will produce different pairing results. Of course, both strategies can make a contribution in performance enhancement compared with the conventional pairwise PEE [25], and the improvements are verified in experimental results in Section IV.

B. Adaptive mapping selection

There is no question that a RDH method can be represented as a reversible mapping Θ. Consider a n-dimensional space, the general form of Θ can be defined as : $\mathbf{Z}^n \rightarrow P(\mathbf{Z}^n)$ where $P(\mathbf{Z}^n)$ is the power set of $\mathbf{Z}^n$ [38]. The reversibility requires that $\Theta(x) \cap \Theta(y) = \emptyset$ holds for any $x \neq y$ and $x, y \in \mathbf{Z}^n$. Because there exist various mappings, defining of the optimal mapping naturally becomes the key concern of RDH which depends both on the employed PEH and the required capacity. For a given n-dimensional PEH, the optimal mapping Θ^* is determined to fulfill the following objective

$$\begin{cases} \Theta^* = \arg\min \frac{ED}{EC} \\ \text{subject to} \quad EC \geq PS \end{cases} \tag{10}$$

where EC and ED are the derived capacity and the embedding distortion, and PS is the required payload size. According the specific mapping, the calculations of EC and ED on the 2D PEH could be referred to [25], and are omitted here for simplicity. Intuitively, the mapping in [25] is just a special case in the 2D space, and may not be suitable for different PEHs. A better 2D mapping should be designed depending upon the characteristic of the PEH. In our method, since the 1D PEH is modified by the conventional 1D mapping, we only need to optimize the mapping for the 2D PEH. The proposed 2D PEH is special, and only consists of the small-magnitude prediction-errors. In the first quadrant, there are four 2D bins including $(0,0), ..., (1,1)$. Hence, the optimization is just to modify the four bins, and many variations can be obtained in the combination of their modifications. We give three solutions for the 2D mapping selection including one fixed mapping selection and two adaptive mapping selections, each of which can be used in the hybrid data embedding to yield a better performance than [25].

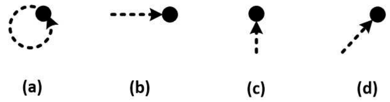

Fig. 11. Four possible inputs for a 2D bin.

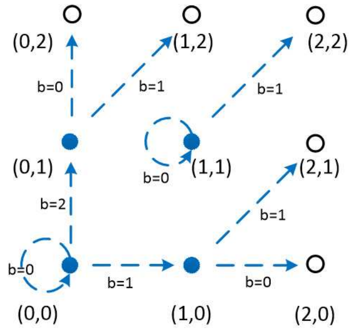

Fig. 12. The input choices for the 2D bins in the first quadrant. As a result, we can derive 336 different feasible 2D mappings.

1) Fixed mapping selection (FM): In this solution, the same 2D mapping in [25] is adopted for the data embedding of smooth set S, which is constant for all images. The pixels in $S_{(-2,1)}$ are paired up, and then modified in the manner as shown in Fig. 12. The only difference from [25] is the histogram generation. Here, by rejecting the large-magnitude prediction-errors for the 2D PEH, the 2D mapping is limited in the small range and the void circle in the figure represents that the number of the pair is zero. The rest of pixels in the image are classified into the set R, and are added or subtracted by 1, respectively. As the fixed mapping is used, we do not need to solve the optimization (10), and so this solution gives a fast processing speed.

2) Adaptive mapping selection using generic search (AMG): For the adaptive mapping selection, the direct solution is to enumerate all the variants and find the best result using (10). However, this is very time-consuming. So, we consider to simplify the optimization by introducing some constraint, and call this solution for optimization as the generic search. In the mapping, we modify the input of a 2D bin to obtain its

This article has been accepted for publication in a future issue of this journal, but has not been fully edited. Content may change prior to final publication. Citation information: DOI 10.1109/TCSVT.2018.2859792, IEEE Transactions on Circuits and Systems for Video Technology

variation. The possible input for a 2D bin is defined as

$$\Theta_{\text{input}}(k_1, k_2) = \{(c_1, c_2) : c_i \in g(k_i), i \in \{1, 2\}\} \tag{11}$$

where $g : \mathbf{Z} \rightarrow P(\mathbf{Z})$ is a function constrained by $|x - g(x)| \leq 1$. It denotes where a marked 2D bin can be mapped from. We can enumerate the possible inputs as the variations for a 2D bin, and then generate a complete mapping once the inputs of 2D bins are determined. It is easily induced that the mapping is reversible if and only if each 2D bin has one input. Otherwise, there is an ambiguity for data recovery. Based on the above definition, the constraint on the variation of a 2D bin is defined as follows.

- For an efficient 2D mapping, the high-occurrence 2D bin could be mapped to a low-occurrence one, but the mapping from the low-occurrence one to the high-occurrence one is prohibited.

This can be best understood through the comparison with the movement of water, i.e., the water always flows down into the nearest low terrain. Taking the first quadrant of 2D PEH for illustration, the marked pair (k_1', k_2') can only be mapped from the four 2D values, i.e.,

$$(k_1', k_2') = \begin{cases} (k_1, k_2), & \text{if case (a)} \\ (k_1 - 1, k_2), & \text{if case (b)} \\ (k_1, k_2 - 1), & \text{if case (c)} \\ (k_1 - 1, k_2 - 1), & \text{if case (d)} \end{cases} \tag{12}$$

because that the 2D PEH is a Laplacian-like distribution centered at $(0, 0)$ and the occurrences of these neighbors are higher than that of (k_1, k_2). In this case, only four possible input choices are available for a 2D bin (k_1, k_2) as shown in Fig.11. Referring to (11), we have $\Theta_{\text{input}}(k_1', k_2') = \{(k_1, k_2), (k_1 - 1, k_2), (k_1, k_2 - 1), (k_1 - 1, k_2 - 1)\}$. Similarly, the other three quadrants adopt the same philosophy for the variations. The inputs of 9 bins $(0, 0)$, ..., $(2, 2)$ in the first quadrant construct the complete 2D mapping for the four bins $(0, 0)$, ..., $(1, 1)$. One can obtain the possible input choices for each bin as shown in Fig. 13, and the number of candidate 2D mappings in theory is 432. In the figure, the number in the circle denotes the possible choices for the 2D bin. For instance, $\Theta_{\text{input}}(0, 0) = \{(0, 0)\}$ and $\Theta_{\text{input}}(1, 1) = \{(0, 0), (0, 1), (1, 0), (1, 1)\}$, then the numbers of choice are $\#\Theta_{\text{input}}(0, 0) = 1$ and $\#\Theta_{\text{input}}(1, 1) = 4$. However, some candidates are irreversible, in which at least one 2D bin is assigned with more than one input. So, by further eliminating these invalid mappings, the actual candidate number is only 336. The solution space is not large, and thus the optimization in (10) can be solved within an acceptable cost by exhaustively enumerating all candidate mappings.

After generating the PEH, the optimal mapping is determined by solving the optimization (10). Compared with the conventional pairwise PEE with a fixed mapping, the proposed method supports more choices for adaptive embedding, and thus has a potential for better performance. To show the adaptivity of the proposed method, we compare the optimal 2D mapping determined by (10) on different images. Fig. 14 shows the occurrences of 2D bins in the first quadrant of 2D PEH in our method, and gives the optimal mapping correspondingly for 10,000 bits. From Fig. 14, one can see that

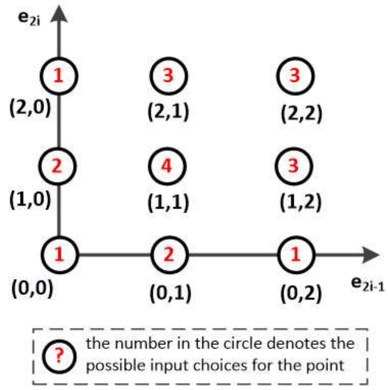

Fig. 13. The input choices for the 2D bins in the first quadrant. As a result, there are 432 different combinations.

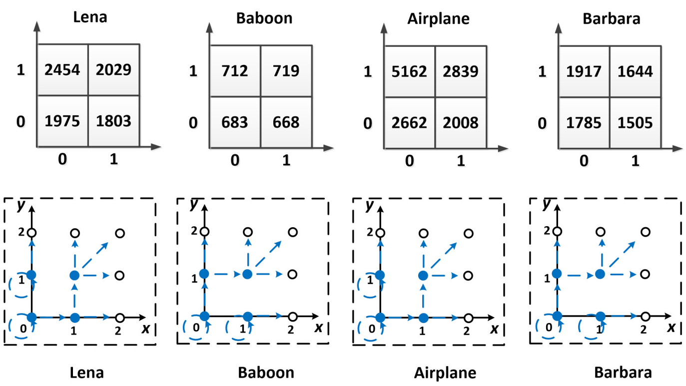

Fig. 14. The occurrences of 2D bins in the first quadrant by using the proposed method and the corresponding optimal 2D mapping using AMG.

the proposed 2D mappings are different from that of pairwise PEE, and each has its own speciality based on the PEH. Here, the threshold in the example is set as maximum to include all the prediction-errors in $S_{(-2,1)}$.

3) Adaptive mapping selection using optimal transition probability matrix (AMO): The third solution is to design the best 2D mapping by using the optimization algorithm, which aims at analyzing the property of the problem and solves it without the exhaustive search. In the past, a large effort of watermarking community has gone into developing methods for solving optimal embedding. For a spread-spectrum watermarking, the classical optimal embedding is to determine the modification amplitude for the host signal adaptively, so as to minimize the bit-error-rate for a given distortion level at receivers [39], [40]. It is formulated as the trade-off between the average bit-error-rate of secret messages and a total distortion constraint. Slightly different from that, the optimality of RDH is to minimize the distortion with a constraint of capacity requirement. Here, our solution is based on the recent technique of optimal transition probability matrix (OTPM), which is proposed by Zhang *et al.* [13]. The work [13] provides a more efficient mechanism for optimizing the data embedding of long term cover sequence, and the optimal data embedding is formulated as a rate-distortion minimization

This article has been accepted for publication in a future issue of this journal, but has not been fully edited. Content may change prior to final publication. Citation information: DOI 10.1109/TCSVT.2018.2859792, IEEE Transactions on Circuits and Systems for Video Technology

TABLE III
THE OPTIMAL TRANSITION MATRIX OF LENA USING AMO FOR THE CAPACITY OF 10,000 BITS. HERE, ONLY THE PIXELS OF THE FIRST LAYER ARE USED FOR THE TEST.

X/Y	(0,0)	(0,1)	(0,2)	(1,0)	(1,1)	(1,2)	(2,0)	(2,1)	(2,2)
(0,0)	0.5720	0.1823	0	0.1701	0.0756	0	0	0	0
(0,1)	0	0.3409	0.4417	0	0.1020	0.1153	0	0	0
(1,0)	0	0	0	0.3384	0.1229	0	0.4169	0.1217	0
(1,1)	0	0	0	0	0.1358	0.2814	0	0.2629	0.3199

TABLE IV
THE OPTIMAL TRANSITION MATRIX OF LENA USING AMO FOR THE CAPACITY OF 20,000 BITS. HERE, ONLY THE PIXELS OF THE FIRST LAYER ARE USED FOR THE TEST.

X/Y	(0,0)	(0,1)	(0,2)	(1,0)	(1,1)	(1,2)	(2,0)	(2,1)	(2,2)
(0,0)	0.4902	0.2072	0	0.2065	0.0961	0	0	0	0
(0,1)	0	0.2624	0.4446	0	0.0964	0.1966	0	0	0
(1,0)	0	0	0	0.2625	0.0956	0	0.4431	0.1988	0
(1,1)	0	0	0	0	0.1623	0.2225	0	0.2185	0.3968

problem as

$$\begin{cases} \text{minimize} & \sum_x \sum_y P_X(x)P_{Y|X}(y|x)D(x,y) \\ \text{subject to} & -\sum_y P_Y(y)\log_2(P_Y(y)) \geq H_Y \\ & \sum_x P_X(x)P_{Y|X}(y|x) = P_Y(y), \forall y \\ & \sum_y P_{Y|X}(y|x) = 1, \forall x \\ & P_{Y|X}(y|x) \geq 0, \forall x, y \end{cases} \tag{13}$$

where X and Y are the cover and the marked sequences, $H(\cdot)$ denotes the entropy function, $P_{Y|X}(y|x)$ is the transition possibility matrix, $P(\cdot)$ denotes the possibility distribution, and $D(x, y)$ returns the Euclidian distance between the corresponding two pairs of x and y. In our method, the cover sequence X is generated from $S_{(-2,1)}$, and the derived marked sequence ranges from $-3 \leq e'_{2i-1}, e'_{2i} \leq 2$. According to [13], we first transform the 2D cover sequence into a 1D one, by projecting each 2D prediction-error pair (e_{2i-1}, e_{2i}) into a 1D value $\tilde{e}_i$ as

$$\tilde{e}_i = (e_{2i-1} + 3) \times 6 + (e_{2i} + 3). \tag{14}$$

The projection here is slightly different from [13] because the lower and upper bounds of the to-be-optimized prediction-errors in the marked sequence are symmetrically set as $[-3, 2]$. By counting the possibility distribution P_X, we use the OTPM to determine the optimal modification from X to Y. Note that in X, the possibilities for the void bins (i.e., the 2D bin contains at least one prediction-error with the value of -3 or 2) are zero-valued. Tables. III and IV show the corresponding OTPMs of Lena for the capacities of 10,000 and 20,000 bits respectively, where only the transition possibilities for the first quadrant of 2D PEH are given.

In summary, based on our experimental results (see Section IV), the above three solutions can enhance the conventional pairwise PEE, and the two adaptive solutions obtain the better results. The merit of the two adaptive solutions is that the 2D modification is adaptive for the PEH. Of course, the PEH is not just determined by the image, but also related to the noise level threshold. So, the threshold is another parameter for data embedding. For a given capacity, in each solution, the strategy for the determination of threshold is to first enumerate all the thresholds of noise level, and then select the one to achieve the best embedding performance.

IV. EXPERIMENTAL RESULTS AND DISCUSSIONS

In this section, we study the performance of the proposed method by comparing it with the conventional pairwise PEE [25] and three other state-of-the-art methods [17], [27], [28]. In the experiment, the two layers are equally embedded with a half size of payload, and the higher-dimensional mapping of each layer will be optimized by the adaptive mapping selection. After the first layer is embedded, its marked pixels are then taken as the context for the second layer. In addition, as three different high-dimensional implementations (i.e., FM, AMG and AMO) are considered, the proposed method using the three solutions for 2D modification in III-B are denoted as Pro-FM, Pro-AMG and Pro-AMO, respectively.

We first compare the overall embedding performance for different embedding rates (the unit is bit per pixel, and abbreviated to BPP), and two comparisons are conducted on six standard images with size of 512×512. The first comparison between Pro-AMO with the counterparts is reported in Fig. 15, and the other comparison for the proposed method using three different mapping selections (i.e., Pro-FM, Pro-AMG and Pro-AMO) is plotted in Fig. 16. It is seen from Fig. 15 that Pro-AMO can outperform the conventional pairwise PEE [25] and the other compared methods. Our gain over the previous works is mainly due to the low-entropy PEHs and the adaptive mapping selection. Besides, it is observed that the consistent gain can also be obtained over the improved pairwise PEE with APP stragegy [28]. The average gain of Pro-AMO over [28] is 0.53 dB on the test images for different embedding rates. It is demonstrated that the proposed APP combined with adaptive mapping selection can make a further enhancement. From Fig. 16, we can see that Pro-AMG and Pro-AMO both yield a higher PSNR than Pro-FM. By simply using the hybrid embedding without the adaptive modification, the proposed method Pro-FM can also improve the conventional pairwise PEE. The details of comparison for the capacities of 10,000 and 20,000 bits are given in Table V and VI, respectively. As shown in the tables, the average performance of the proposed method is the best. For 10,000 and 20,000 bits, the average PSNR gains by Pro-FM over [25] are 0.43 and 0.24 dB, respectively. By using the adaptive 2D mapping, the

TABLE V
COMPARISON OF PSNR FOR THE CAPACITY OF 10,000 BITS, WHERE THE UNIT IS dB.

Images	[17]	[27]	[25]	[28]	Pro-FM	Pro-AMG	Pro-AMO
Lena	58.20	60.10	59.75	59.89	60.02	60.42	60.77
Baboon	54.16	55.21	55.21	55.72	55.76	56.00	56.10
Airplane	60.40	62.43	63.76	63.84	63.79	64.15	65.08
Barbara	58.15	60.66	59.48	59.94	59.91	60.50	60.58
Lake	56.66	59.93	58.72	59.02	58.47	59.11	59.35
Boat	56.14	57.42	57.55	58.04	57.95	58.15	58.41
Average	57.29	59.29	59.08	59.40	59.32	59.72	60.05

TABLE VI
COMPARISON OF PSNR FOR THE CAPACITY OF 20,000 BITS, WHERE THE UNIT IS dB.

Images	[17]	[27]	[25]	[28]	Pro-FM	Pro-AMG	Pro-AMO
Lena	55.04	56.59	56.29	56.42	56.52	57.00	57.25
Baboon	49.39	49.84	50.12	51.18	51.22	51.28	51.69
Airplane	57.32	59.51	60.20	60.35	60.22	60.54	61.41
Barbara	55.04	57.11	56.27	56.65	56.56	57.10	57.24
Lake	52.71	53.17	53.76	54.31	54.22	54.30	54.66
Boat	52.65	53.52	53.34	53.94	53.86	54.08	54.40
Average	53.71	54.95	55.00	55.48	55.43	55.72	56.11

corresponding gains by Pro-AMG and Pro-AMO are 0.72 and 1.07 dB for 10,000 bits, respectively, and the improvements for 20,000 bits are 0.64 and 1.11 dB, respectively. Compared with the latest pairwise PEE-based method [28], our average gains obtained by Pro-AMO are 0.65 and 0.73 dB for the capacities of 10,000 an 20,000 bits, respectively. The method [28] performs slightly better than Pro-FM. It is indicated that the similarities of both distance and intensity can be further exploited to improve the histogram generation. The stable gain for the complex texture image, such as Baboon, confirms that our method is content-based embedding and therefore can yield a better performance on the relatively complex images on which the conventional methods cannot work well.

In order to demonstrate the performance of adaptive mapping selection, we present the optimal mapping in (10) on a given PEH. In the hybrid PEH, only the higher-dimensional mapping needs to be optimized, and the 1D mapping is constant. So, we merely investigate the optimal mapping for the high-dimensional PEH. The employed high-dimensional PEH is determined by two parameters, i.e., the image and the required capacity. We fix one parameter when investigating the other one, and take the histogram modification of Pro-AMG for illustration. The optimal 2D mappings of two layers are given in Fig. 17 for different cases. The proposed 2D mapping can be adaptive to the characteristic of PEH, which is quite different from the conventional 2D mapping in [25]. It is due that the 2D mappings of both two layers are optimized.

In order to demonstrate the embedding performance with respect to the structural change between the original image

TABLE VII
PERFORMANCE COMPARISON IN TERMS OF SSIM. THE SYMBOL "-" DENOTES THAT THE CORRESPONDING METHOD CANNOT FULFILL THE CAPACITY.

Methods	Capacity BPP	Lena	Baboon	Airplane	Barbara	Lake	Boat
Pro-AMG	0.1	0.9997	-	0.9998	0.9998	0.9997	0.9997
	0.2	0.9996	-	0.9996	0.9996	-	-
Pro-AMO	0.1	0.9997	-	0.9998	0.9998	0.9997	0.9997
	0.2	0.9996	-	0.9996	0.9997	-	-
Pro-FM	0.1	0.9997	-	0.9998	0.9998	0.9997	0.9997
	0.2	0.9995	-	0.9996	0.9996	-	-
[17]	0.1	0.9997	0.9995	0.9997	0.9997	0.9997	0.9996
	0.2	0.9994	0.9983	0.9995	0.9994	0.9990	0.9991
[27]	0.1	0.9999	0.9996	0.9999	0.9999	0.9999	0.9999
	0.2	0.9998	0.9986	0.9999	0.9998	0.9996	0.9997
[25]	0.1	0.9997	-	0.9998	0.9998	0.9997	0.9997
	0.2	0.9995	-	0.9996	-	-	-
[28]	0.1	0.9994	-	0.9997	0.9996	0.9997	0.9995
	0.2	0.9991	-	0.9995	0.9994	-	-

TABLE VIII
THE PERFORMANCE COMPARISON (PSNR IN dB) FOR A CAPACITY OF 10,000 BITS UNDER ADDITIVE WHITE GAUSSIAN NOISE, WHERE THE NOISE PARAMETERS ARE SET AS MEAN = 0, VARIANCE = 0.01, 0.03. THE SYMBOL "-" DENOTES THAT THE CORRESPONDING METHOD CANNOT FULFILL THE CAPACITY.

Methods	Gaussian noise Variance	Lena	Baboon	Airplane	Barbara	Lake	Boat
Pro-AMG	0.01	52.55	51.48	52.7	52.48	52.02	52.11
	0.03	50.05	49.23	50.1	49.88	49.76	49.81
Pro-AMO	0.01	52.53	51.52	52.68	52.52	52.06	52.11
	0.03	50.72	49.29	50.13	49.92	49.80	49.86
Pro-FM	0.01	52.41	51.36	52.55	52.36	51.89	52.00
	0.03	49.98	49.13	49.99	49.8	49.67	49.73
[17]	0.01	51.64	50.23	51.68	51.39	50.99	51.07
	0.03	49.17	46.52	49.16	48.86	48.73	48.59
[27]	0.01	54.33	51.19	54.40	53.38	53.35	53.45
	0.03	50.86	48.68	50.53	49.64	49.87	49.53
[25]	0.01	51.79	50.58	51.92	51.75	51.27	51.34
	0.03	49.33	-	49.27	49.05	48.93	48.93
[28]	0.01	52.19	51.2	52.68	52.21	51.79	51.88
	0.03	49.72	49.13	50.11	49.83	49.56	49.70

and the marked one, we use the structural similarity index (SSIM) [41] to make a further comparison as shown in Table VII. Here, we compare the SSIM performance for a relative high embedding rate of our method, i.e., 0.1 and 0.2 BPP, respectively. From the table, we can see that the listed methods can all provide a very high SSIM value, and the image structure is well preserved after data embedding. The reason is given as follows. On one hand, the proposed method is a high-fidelity algorithm where the maximum modification on a pixel is 1, and therefore the degradation of image is limited. On the other hand, unlike the watermarking scheme, RDH does not attempt to change the image structure, and tends to modify the pixels in smooth regions preferentially and keep the rough pixels less modified.

To examine the performance for the practical scenario, we

This article has been accepted for publication in a future issue of this journal, but has not been fully edited. Content may change prior to final publication. Citation information: DOI 10.1109/TCSVT.2018.2859792, IEEE Transactions on Circuits and Systems for Video Technology

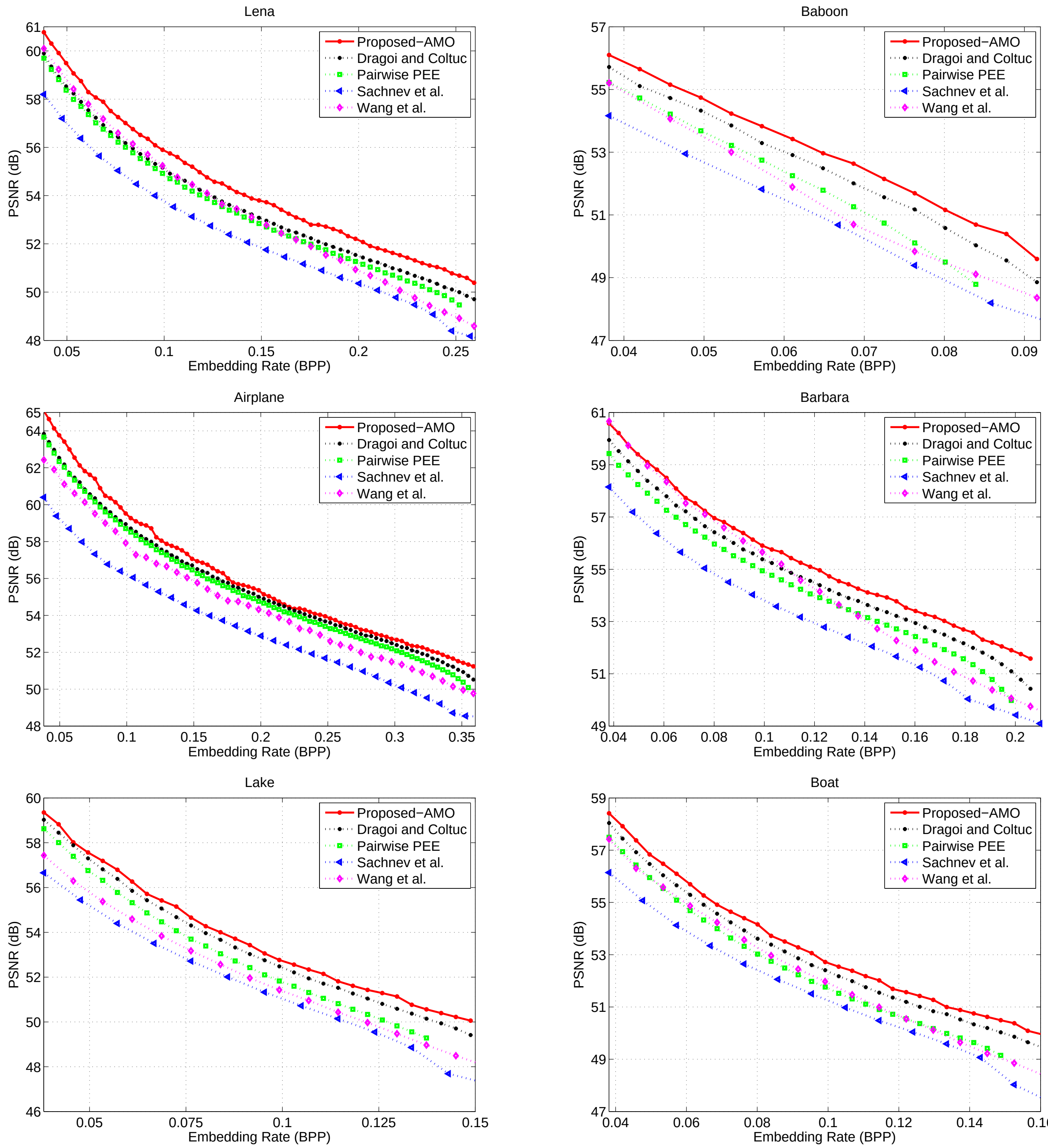

Fig. 15. Performance comparisons in terms of capacity-distortion trade-off.

conduct the comparisons on the degraded images as shown in Tables VIII and IX. Here, the degraded image is obtained by applying two common noises respectively on the standard image, including the additive white Gaussian noise and the salt & peppers noise. The two noises are often used to stimulate the practical environment, such as satellite and deep space communication. Besides, they are mathematically tractable to give insight into the algorithm. The PSNR is evaluated between the original image and the marked noisy one. In the stimulation, as shown in Table VIII, the Gaussian noise is parameterized with the mean = 0, and its variance is set as 0.01 or 0.03. For the salt & peppers noise, the corrupted probability of a pixel is set as 0.01 or 0.03 as shown in Table IX. It is found that the proposed method is more sensitive to the noise, and the performance gain of Pro-AMO over Pro-AMG and Pro-FM diminishes. Obviously, the high-fidelity embedding of our method relies on the high correlation of neighboring pixels. As the correlations are destructed, the advantage of adaptive embedding is reduced. It is noted that our method can still provide a better embedding performance compared with the

This article has been accepted for publication in a future issue of this journal, but has not been fully edited. Content may change prior to final publication. Citation information: DOI 10.1109/TCSVT.2018.2859792, IEEE Transactions on Circuits and Systems for Video Technology

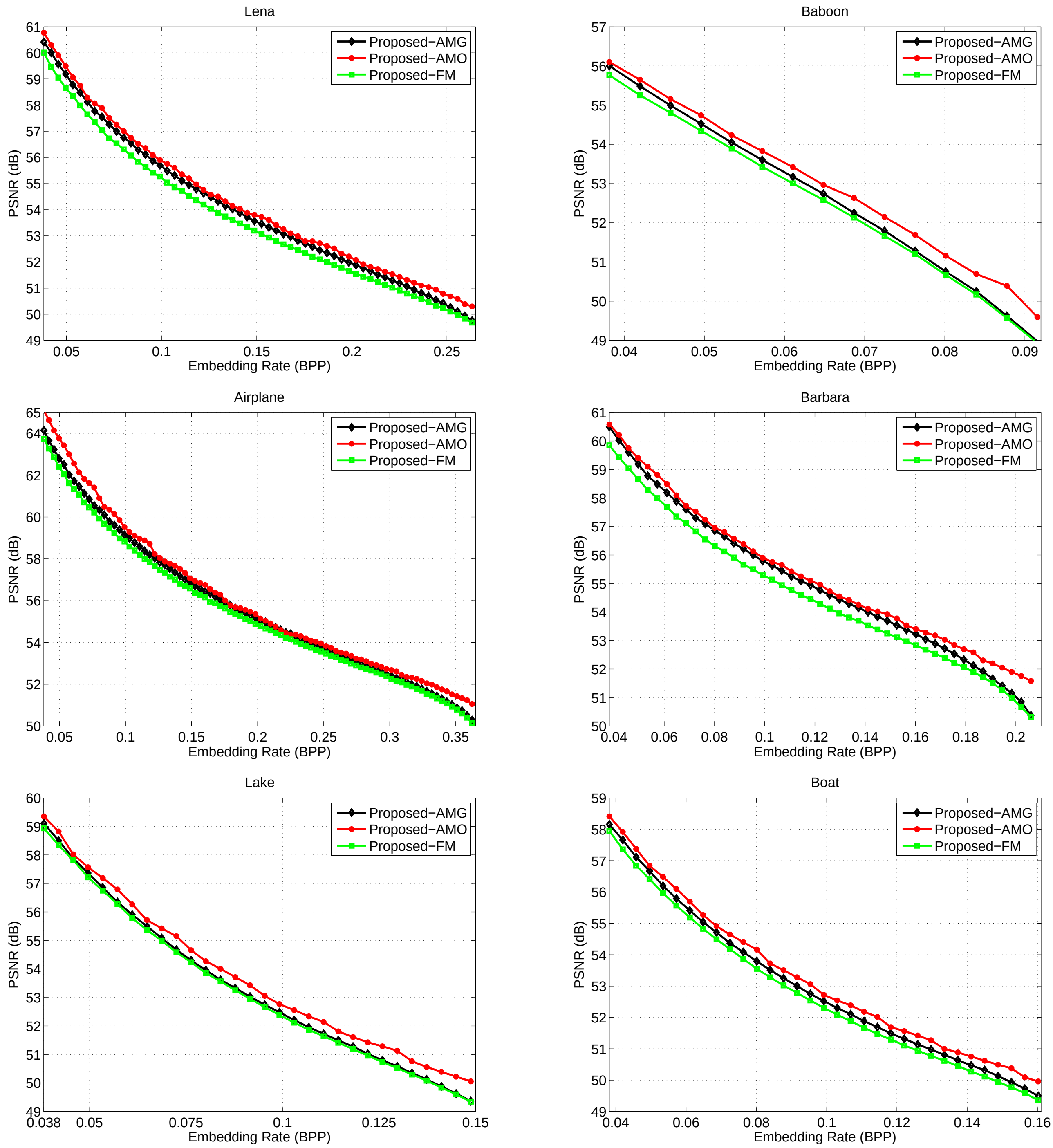

Fig. 16. Performance comparisons of the proposed method using three mapping strategies, including FM, AMG and AMO.

methods [17], [25], [28], and the method [27] yields the best result in this case.

At last, for the computational complexity, the cost of the proposed method is not expensive. By using the accelerating technique, the runtime of once embedding for Pro-AMG and Pro-AMO are 18 and 64 seconds respectively on average, where the method is implemented by Matlab and on a personal PC.

V. Conclusion

In this paper, we propose a new implementation for the design of high-dimensional RDH, which is based on the hybrid histogram generation and the adaptive mapping selection. For the histogram generation, we use the APP to classify the prediction-errors into the smooth and rough sets, and derive the high-dimensional PEH by only combining the small-magnitude prediction-errors. We show that the hybrid PEH is more helpful for RDH with a lower entropy than the conventional single 2D PEH. For histogram modification, the

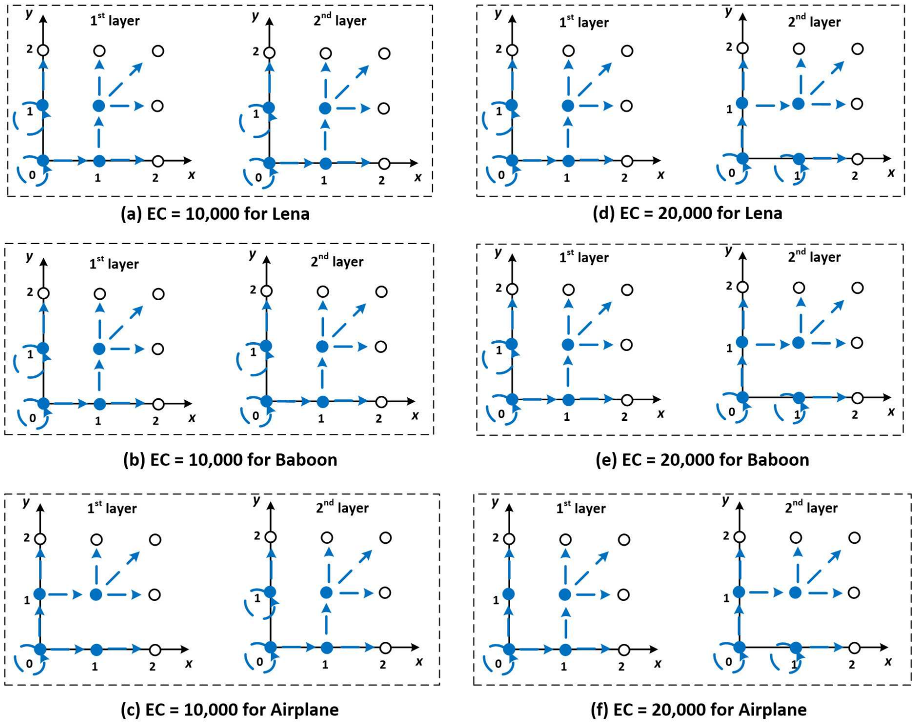

Fig. 17. Optimal 2D mapping using Pro-AMG for different capacities. In each case, two mappings for the double layers are all given.

TABLE IX
THE PERFORMANCE COMPARISON (PSNR IN dB) FOR A CAPACITY OF 10,000 BITS UNDER THE SALT AND PEPPERS NOISE, WHERE THE CORRUPTED PROBABILITIES ARE SET AS 0.01 AND 0.03, RESPECTIVELY.

Methods	Salt-peppers probability	Lena	Baboon	Airplane	Barbara	Lake	Boat
Pro-AMG	0.01	60.03	55.78	63.28	60.11	58.71	57.88
	0.03	59.38	55.37	61.99	59.35	57.90	57.22
Pro-AMO	0.01	60.37	55.92	64.77	60.28	58.84	58.02
	0.03	59.38	55.37	61.99	59.35	57.90	57.22
Pro-FM	0.01	59.57	55.56	63.01	59.57	58.59	57.61
	0.03	59.00	55.19	61.78	58.90	57.82	57.02
[17]	0.01	58.07	53.74	60.25	58.02	56.37	55.83
	0.03	57.68	52.28	60.05	57.64	55.68	55.17
[27]	0.01	60.09	55.15	61.91	60.60	57.24	57.35
	0.03	59.98	54.93	61.79	60.50	57.13	57.10
[25]	0.01	58.82	54.83	61.92	58.61	57.83	56.85
	0.03	57.53	54.13	59.59	57.47	56.58	55.92
[28]	0.01	59.27	55.33	62.81	59.61	58.62	57.43
	0.03	58.92	55.03	61.78	58.81	57.82	57.12

corresponding high-dimensional mapping is adaptively chosen to make the data embedding well suited to the derived PEH. The proposed method is tested on the standard images, and the two adaptive modifications for the high-dimensional PEH based on generic search and OTPM are implemented. All the experimental results demonstrates the consistent performance gains by using our method, some of which are significant.

REFERENCES

[1] Y. Q. Shi, X. Li, X. Zhang, H. T. Wu, and B. Ma, "Reversible data hiding: Advances in the past two decades," *IEEE Access*, vol. 4, pp. 3210–3237, 2016.

[2] M. U. Celik, G. Sharma, A. M. Tekalp, and E. Saber, "Lossless generalized-LSB data embedding," *IEEE Trans. Image Process.*, vol. 14, no. 2, pp. 253–266, 2005.

[3] W. Zhang, X. Hu, X. Li, and N. Yu, "Recursive histogram modification: Establishing equivalency between reversible data hiding and lossless data compression," *IEEE Trans. Image Process.*, vol. 22, no. 7, pp. 2775–2785, 2013.

[4] X. Zhang, "Separable reversible data hiding in encrypted image," *IEEE Trans. Inf. Forens. Security*, vol. 7, no. 2, pp. 826–832, 2012.

[5] ——, "Reversible data hiding with optimal value transfer," *IEEE Trans. Multimedia*, vol. 15, no. 2, pp. 316–325, 2013.

[6] Z. Qian and X. Zhang, "Reversible data hiding in encrypted images with distributed source encoding," *IEEE Trans. Circuits Syst. Video Technol.*, vol. 26, no. 4, pp. 636–646, 2016.

[7] F. Huang, X. Qu, H. J. Kim, and J. Huang, "Reversible data hiding in JPEG images," *IEEE Trans. Circuits Syst. Video Techn.*, vol. 26, no. 9, pp. 1610–1621, 2016.

[8] Z. Ni, Y. Q. Shi, N. Ansari, and W. Su, "Reversible data hiding," *IEEE Trans. Circuits Syst. Video Technol.*, vol. 16, no. 3, pp. 354–362, Mar. 2006.

[9] P. Tsai, Y. C. Hu, and H. L. Yeh, "Reversible image hiding scheme using predictive coding and histogram shifting," *Signal Processing*, vol. 89, no. 6, pp. 1129–1143, 2009.

[10] H.-T. Wu and J. Huang, "Reversible image watermarking on prediction errors by efficient histogram modification," *Signal Processing*, vol. 92, no. 12, pp. 3000–3009, 2012.

[11] X. Li, B. Li, B. Yang, and T. Zeng, "General framework to histogram-shifting-based reversible data hiding," *IEEE Trans. Image Process.*, vol. 22, no. 6, pp. 2181–2191, 2013.

[12] ——, "General framework to histogram-shifting-based reversible data hiding," *IEEE Trans. Image Process.*, vol. 22, no. 6, pp. 2181–2191, 2013.

[13] W. Zhang, X. Hu, X. Li, and Y. Nenghai, "Optimal transition probability of reversible data hiding for general distortion metrics and its applications," *IEEE Trans. Image Process.*, vol. 24, no. 1, pp. 294–304, 2015.

[14] J. Tian, "Reversible data embedding using a difference expansion," *IEEE Trans. Circuits Syst. Video Technol.*, vol. 13, no. 8, pp. 890–896, 2003.

[15] X. Li, W. Zhang, X. Gui, and B. Yang, "A novel reversible data hiding scheme based on two-dimensional difference-histogram modification," *IEEE Trans. Inf. Forens. Security*, vol. 8, no. 7, pp. 1091–1100, 2013.

This article has been accepted for publication in a future issue of this journal, but has not been fully edited. Content may change prior to final publication. Citation information: DOI 10.1109/TCSVT.2018.2859792, IEEE Transactions on Circuits and Systems for Video Technology

[16] D. M. Thodi and J. J. Rodriguez, “Expansion embedding techniques for reversible watermarking,” *IEEE Trans. Image Process.*, vol. 16, no. 3, pp. 721–730, 2007.

[17] V. Sachnev, H. J. Kim, J. Nam, S. Suresh, and Y. Q. Shi, “Reversible watermarking algorithm using sorting and prediction,” *IEEE Trans. Circuits Syst. Video Technol.*, vol. 19, no. 7, pp. 989–999, 2009.

[18] G. Coatrieux, C. L. Guilou, J.-M. Cauvin, and C. Roux, “Reversible watermarking for knowledge digest embedding and reliability control in medical images,” *IEEE Trans. Inf. Techn. in Biomedicine*, vol. 13, no. 2, pp. 158–165, 2009.

[19] H. J. Hwang, H. Kim, V. Sachnev, and S. Joo, “Reversible watermarking method using optimal histogram pair shifting based on prediction and sorting,” *KSII Transactions on Internet and Information Systems*, vol. 4, no. 4, pp. 655–670, 2010.

[20] X. Gao, L. An, Y. Yuan, D. Tao, and X. Li, “Lossless data embedding using generalized statistical quantity histogram,” *IEEE Trans. Circuits Syst. Video Technol.*, vol. 21, no. 8, pp. 1061–1070, 2011.

[21] X. Li, B. Yang, and T. Zeng, “Efficient reversible watermarking based on adaptive prediction-error expansion and pixel selection,” *IEEE Trans. Image Process.*, vol. 20, no. 12, pp. 3524–3533, 2011.

[22] W. Hong, “Adaptive reversible data hiding method based on error energy control and histogram shifting,” *Optics Communications*, vol. 285, no. 2, pp. 101–108, 2012.

[23] G. Coatrieux, W. Pan, N. Cuppens-Boulahia, F. Cuppens, and C. Roux, “Reversible watermarking based on invariant image classification and dynamic histogram shifting,” *IEEE Trans. Inf. Forens. Security*, vol. 8, no. 1, pp. 111–120, 2013.

[24] C. Qin, C.-C. Chang, Y.-H. Huang, and L.-T. Liao, “An inpainting-assisted reversible steganographic scheme using histogram shifting mechanism,” *IEEE Trans. Circuits Syst. Video Techn.*, vol. 23, no. 7, pp. 1109–1118, 2013.

[25] B. Ou, X. Li, Y. Zhao, R. Ni, and Y.-Q. Shi, “Pairwise prediction-error expansion for efficient reversible data hiding,” *IEEE Trans. Image Process.*, vol. 22, no. 12, pp. 5010–5021, 2013.

[26] X. Wang, J. Ding, and Q. Pei, “A novel reversible image data hiding scheme based on pixel value ordering and dynamic pixel block partition,” *Information Sciences*, vol. 310, no. 0, pp. 16 – 35, 2015.

[27] J. Wang, J. Ni, X. Zhang, and Y.-Q. Shi, “Rate and distortion optimization for reversible data hiding using multiple histogram shifting,” *IEEE Trans. Cybernetics*, vol. PP, no. 99, pp. 1–12, 2016.

[28] I. C. Dragoi and D. Coltuc, “Adaptive pairing reversible watermarking,” *IEEE Trans. Image Process.*, vol. 25, no. 5, pp. 2420–2422, 2016.

[29] C. Qin, X. Chen, D. Ye, J. Wang, and X. Sun, “A novel image hashing scheme with perceptual robustness using block truncation coding,” *Information Sciences*, vol. 361-362, no. Supplement C, pp. 84 – 99, 2016.

[30] C. Qin, P. Ji, X. Zhang, J. Dong, and J. Wang, “Fragile image watermarking with pixel-wise recovery based on overlapping embedding strategy,” *Signal Processing*, vol. 138, pp. 280–293, 2017.

[31] D. Coltuc and J. M. Chassery, “Very fast watermarking by reversible contrast mapping,” *IEEE Signal Process. Lett.*, vol. 14, no. 4, pp. 255–258, 2007.

[32] S. Weng, Y. Zhao, J. S. Pan, and R. Ni, “Reversible watermarking based on invariability and adjustment on pixel pairs,” *IEEE Signal Process. Lett.*, vol. 15, pp. 721–724, 2008.

[33] X. Wang, X. Li, B. Yang, and Z. Guo, “Efficient generalized integer transform for reversible watermarking,” *IEEE Signal Process. Lett.*, vol. 17, no. 6, pp. 567–570, 2010.

[34] F. Peng, X. Li, and B. Yang, “Adaptive reversible data hiding scheme based on integer transform,” *Signal Processing*, vol. 92, no. 1, pp. 54–62, 2012.

[35] C. Wang, X. Li, and B. Yang, “Efficient reversible image watermarking by using dynamical prediction-error expansion,” in *Proc. IEEE ICIP*, 2010, pp. 3673–3676.

[36] G. Xuan, X. Tong, J. Teng, X. Zhang, and Y. Shi, “Optimal histogram-pair and prediction-error based image reversible data hiding,” in *Digital Forensics and Watermaking*, vol. 7809, 2013, pp. 368–383.

[37] X. Li, W. Zhang, X. Gui, and B. Yang, “Efficient reversible data hiding based on multiple histograms modification,” *IEEE Trans. Inf. Forens. Security*, vol. 10, no. 9, pp. 2016 – 2027, 2015.

[38] S. Cai, X. Li, J. Liu, and Z. Guo, “A new reversible data hiding scheme exploiting high-dimensional prediction-error histogram,” in *Proc. IEEE ICIP*, 2016, pp. 2732–2736.

[39] M. Gkizeli, D. A. Pados, and M. J. Medley, “Optimal signature design for spread-spectrum steganography,” *IEEE Transactions on Image Processing*, vol. 16, no. 2, pp. 391–405, 2007.

[40] M. Li, Q. Liu, Y. Guo, B. Wang, and X. Kong, “Amplitude-adaptive spread-spectrum data embedding,” *IET Image Processing*, vol. 10, no. 2, pp. 138–148, 2016.

[41] Z. Wang, A. C. Bovik, H. R. Sheikh, and E. P. Simoncelli, “Image quality assessment: from error visibility to structural similarity,” *IEEE Transactions on Image Processing*, vol. 13, no. 4, pp. 600–612, 2004.

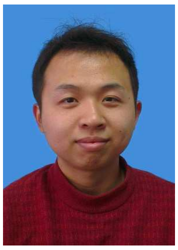

Bo Ou received the B.S. degree and the Ph.D. degree both from Beijing Jiaotong University, Beijing, China, in 2008 and 2014, respectively. After that, he has been a faculty of Hunan University (HNU), Changsha, China. Currently, hs is the assistant professor in HNU. His current research interests include image processing and data hiding.

Xiaolong Li received the B.S. degree from Peking University (China), the M.S. degree from Ecole Polytechnique (France), and the Ph.D. degree in mathematics from ENS de Cachan (France), in 1999, 2002, and 2006, respectively. He worked as a postdoctoral fellow and then a researcher at Peking University in 2007C2016. He is currently a Professor with the Institute of Information Science, Beijing Jiaotong University. His research interests are image processing and information hiding.

Weiming Zhang received his M.S. degree and Ph.D. degree in 2002 and 2005 respectively from Information Engineering University, Zhengzhou, China. Currently, he is a professor with University of Science and Technology of China. His research interests include multimedia security, information hiding, and privacy protection.

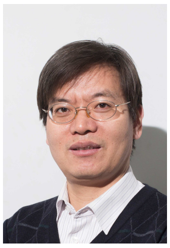

Yao Zhao received the B.S. degree from the Radio Engineering Department, Fuzhou University, Fuzhou, China, in 1989, the M.E. degree from the Radio Engineering Department, Southeast University, Nanjing, China, in 1992, and the Ph.D. degree from the Institute of Information Science, Beijing Jiaotong University (BJTU), Beijing, China, in 1996,where he became an Associate Professor and a Professor in 1998 and 2001, respectively. From 2001 to 2002, he was a Senior Research Fellow with the Information and Communication Theory Group, Faculty of Information Technology and Systems, Delft University of Technology, Delft, The Netherlands. In 2015, he visited the Swiss Federal Institute of Technology, Lausanne (EPFL), Switzerland. From 2017 to 2018, he visited University of Southern California. He is currently the Director with the Institute of Information Science, BJTU. His current research interests include image/video coding, digital watermarking and forensics, video analysis and understanding, and artificial intelligence. Dr. Zhao is a Fellow of the IET. He serves on the Editorial Boards of several international journals, including as an Associate Editor for the IEEE TRANSACTIONS ON CYBERNETICS, a Senior Associate Editor for the IEEE SIGNAL PROCESSING LETTERS, and an Area Editor for Signal Processing: Image Communication. He was named a Distinguished Young Scholar by the National Science Foundation of China in 2010 and was elected as a Chang Jiang Scholar of Ministry of Education of China in 2013.